JOURNAL OF GEOPHYSICAL RESEARCH, VOL. 95, NO. D7, PAGES 10,235–10,247, JUNE 20, 1990

OBSERVED AND MODEL-CALCULATED NO_2/NO RATIOS IN TROPOSPHERIC AIR SAMPLED DURING THE NASA GTE/CITE-2 FIELD STUDY

W.L. Chameides,[1] D.D. Davis,[1] J. Bradshaw,[1] S. Sandholm,[1] M. Rodgers,[1] B. Baum,[1] B. Ridley,[2] S. Madronich,[2] M.A. Carroll,[3] G. Gregory,[4] H.I. Schiff,[5] D.R. Hastie,[5] A. Torres,[6] and E. Condon[7]

Abstract. Data gathered during the NASA GTE/CITE 2 airborne field campaign were analyzed and compared with diagnostically derived parameters to study the NO_x photostationary state in the troposphere and the processes that control this photostationary state. Our analysis focussed on two sets of NO_2/NO ratios derived from the data; these were based on overlapping NO and NO_2 measurements made by two independent techniques; i.e., a chemiluminescent technique and a technique based on two-photon, laser-induced-fluorescence. While for any given 6- to 10-min time interval the two observed NO_2/NO ratios often exhibited significant discrepancies, these discrepancies appeared to be mostly random rather than systematic, and as a result, the average difference for all time intervals with overlapping NO_x measurements was only 12%. One notable exception, however, was the block of data gathered during the last three CITE 2 missions; during these three missions the ratios observed by the chemiluminescent technique were systematically larger than those observed by the laser-induced fluorescence technique by a factor of 1.6. When the data from these three missions were omitted from the analysis, the averages of the observed ratios agreed to within 1%. In contrast to a number of previous studies, the ratios predicted from photochemical model calculations were found to be reasonably consistent with the observed ratios, although on average they tended to fall about 20 - 25% below the observations. This agreement between observations and theory provides strong evidence in support of the importance of peroxy radicals in the fast photochemical cycling of NO_x (and the concomitant photochemical production of O_3) in both the marine and continental troposphere.

Introduction

A fundamental tenet of present-day tropospheric photochemical theory is that the relative levels of tropospheric NO and NO_2 are determined by a rapid cycle of reactions which establish a photostationary state. The simplest description of this photostationary state involves three reactions:

(R1) $\quad NO + O_3 \rightarrow NO_2 + O_2$

which converts NO and O_3 to NO_2 and

(R2) $\quad NO_2 + h\nu \rightarrow NO + O$

(R3) $\quad O + O_2 + M \rightarrow O_3 + M$

which reform NO and O_3 from NO_2. During the daylight hours, (R1), (R2), and (R3) can typically cycle odd nitrogen between NO and NO_2 on a time scale of a few minutes. Because this time scale is considerably shorter than the time scale for NO_x (NO + NO_2) production and destruction, these reactions tend to establish a photostationary state in which the rate of destruction (production) of NO_2 (NO) from (R2) is balanced by NO_2 (NO) production (destruction) from (R1) [Cadle and Johnston, 1952; Leighton, 1961]. Under these conditions, the relative levels of NO_2 and NO are determined by

$$\{[NO_2]/[NO]\}_{pss} = [O_3]\, k_1 / j_2 \qquad (1)$$

where the square brackets denote a species' concentration and k and j denote the rate constant for the appropriate reaction or photolysis, respectively.

A more complete description of the NO_x photostationary state must account for the additional effect of peroxy radical reactions with NO; for example,

(R4) $\quad NO + HO_2 \rightarrow NO_2 + OH$

(R5) $\quad NO + CH_3O_2 \rightarrow NO_2 + CH_3O$

(R6) $\quad NO + RO_2 \rightarrow NO_2 + RO$

(In (R6), R is used to denote an organic radical involving two or more C atoms, such as CH_2CH_2.) These reactions, like (R1), convert NO to NO_2 and lead to a modified expression for the NO_x photostationary state; i.e.,

$$\{NO_2/NO\}_{pss'} = \left([O_3]k_1 + [HO_2]k_4 + [CH_3O_2]k_5 + [RO_2]k_6\right)/j_2 \qquad (2)$$

Note that unlike (R1), the peroxy radical reactions (R4), (R5), and (R6) convert NO to NO_2 without consuming an O_3 molecule and as a result, when followed by (R2) and (R3), act as a net photochemical source of tropospheric O_3. While the difference in the NO_2/NO ratios predicted by equations (1) and (2) appears to be small for conditions typical of the urban atmosphere, it can be quite pronounced in clean air where the ratio of $\{[HO_2] + [CH_3O_2] + [RO_2]\}$ to O_3 tends to be higher [Calvert and Stockwell, 1983; Parrish et al., 1986].

Simultaneous observations of NO, NO_2, O_3, and solar flux in Detroit, Michigan appear to verify the accuracy of equation (1) for conditions typical of urban locations [Stedman and Jackson, 1975]. However, the same has not been true of observations made in less polluted environments [McFarland et al., 1978; Ritter et al., 1979; Fehsenfeld et al., 1983; Parrish et al., 1986; Trainer et al., 1987]. The NO_2/NO ratios observed in nonurban locations have tended to be larger than that predicted by equation (1). Furthermore, with the exception of Trainer et al., these investigators have found that in order to reproduce their observed ratios with equation (2), it was necessary to invoke peroxy radical levels systematically

[1]School of Earth and Atmospheric Sciences, Georgia Institute of Technology, Atlanta.
[2]National Center for Atmospheric Research, Boulder, Colorado.
[3]National Oceanographic and Atmospheric Administration, Boulder, Colorado.
[4]NASA Langley Research Center, Hampton, Virginia.
[5]Department of Chemistry, York University, Downsview, Ontario, Canda.
[6]NASA Wallops Flight Center, Wallops Island, Virginia.
[7]Atmospheric Experiments Branch, NASA Ames Research Center, Moffett Field, California.

Paper number 90JD00249.
0148-0277/90/90JD-00249$05.00

larger than those predicted by simulations using a photochemical model; moreover, the rate of O_3 photochemical production implied by these peroxy radical levels were generally found to be unrealistically large and were not reflected in a commensurate increase in local O_3 levels. There are at least three possible explanations for the apparent inconsistency between the observed NO_2/NO ratios in non urban air and photochemical theory: (1) the measurements were subject to systematic errors, (2) our understanding of NO_x chemistry and/or the processes that control peroxy radicals and O_3 photochemistry is incomplete, or (3) the atmosphere contains significant levels of oxidants, like IO radicals [Chameides and Davis, 1980], which are capable of converting NO to NO_2 without producing O_3.

In this work, data collected during the NASA GTE/CITE 2 field operation [Hoell et al., this issue] are analyzed to shed further light on the problem of the NO_2/NO photostationary state in clean air. Our analysis has two main facets. To obtain an indication of the accuracy with which current technology can measure NO_2/NO ratios in clean air, an intercomparison is made of ratios measured during the field exercise with different instruments using different techniques. To assess the accuracy of present-day tropospheric photochemical theory, each of the measured ratios is also compared with ratios calculated using a photochemical model. (For an additional analysis of NO_2/NO ratios measured during the NASA GTE/CITE field studies the reader is referred to M.A. Carroll et al., (Observed ratios of NO_2/NO contrasted with theoretical calculations: NASA/GTE Cite 1 and GTE/CITE 2, submitted to Journal of Geophysical Research, 1990).

Observed NO_2/NO Ratios

Our intercomparison is based on data gathered during missions 7, 8, 10, 11, 12, 14, 15, and 16 of the GTE/CITE 2 airborne field campaign. (For a complete description of the flight tracks and instrument configuration the reader is referred to Hoell et al., [this issue] and the references cited therein.) We focus primarily on two sets of NO_x measurements, one being the simultaneous NO and NO_2 measurements obtained with the chemiluminescent instrumentation of the National Center for Atmospheric Research and National Oceanic and Atmospheric Administration group, hereinafter referred to as NOCAR [Ridley et al., this issue], and the other being the NO and NO_2 measurements obtained with the photofragmentation two-photon laser-induced-fluorescence (TP-LIF) instrumentation of the Georgia Institute of Technology, hereinafter referred to as GIT [Sandholm et al., this issue].

It should be noted that in addition to the NOCAR and GIT NO_x observations, NO_x measurements were made by two other groups during the CITE 2 campaign. These included chemiluminescent measurements of NO and NO_2 using instrumentation from the Wallops Flight Facility, hereinafter referred to as WFF [Torres, 1985] and NO_2 measurements using a tunable diode laser absorption spectrometer from York University, hereinafter referred to as YU [Schiff et al., this issue]. The WFF NO_2 measurements were not included in our analysis for the same reasons as those cited by Gregory et al., [this issue (a)]. The WFF NO measurements were not included because of the very limited overlap these measurements had with the NOCAR and GIT NO_x measurements. Finally, because the NO_2 levels for most of the daytime CITE 2 flights remained close to the 25 pptv (parts per trillion by volume) detection limit of the YU NO_2 system [Schiff et al., this issue], the YU data were not included in our analysis except for those data gathered during mission 14, when the NO_2 levels were unusually high.

Two sets of NO_2/NO ratios were formed from the NOCAR and GIT NO_x observations: $\{NO_2/NO\}_{NOCAR}$ was obtained by dividing the NOCAR observed NO_2 by the NOCAR observed NO and $\{NO_2/NO\}_{GIT}$ was similarly formed from the GIT NO_2 and NO observations. It should be noted that for conditions typical of the daytime CITE 2 flights (i.e., [NO] ~ 10 - 15 pptv and $[NO_2]$ ~ 20 - 30 pptv), the (1-σ) total uncertainty (combined precision and accuracy) in the NO and NO_2 measurements were 20% for NOCAR NO, 27% for GIT NO, 30% for NOCAR NO_2, and 40% for GIT NO_2 [Gregory et al., this issue (a, b)]. (These uncertainties are based on 1-min and 6-min integration times for the NOCAR and GIT instruments, respectively, and are appropriate for the typical NO and NO_2 concentrations indicated. Larger uncertainties apply for smaller NO_x concentrations, and smaller uncertainties apply for larger concentrations.) If these uncertainties propagated quadratically in the ratio formed from the NO and NO_2 measurements, the uncertainty in the observed ratios would typically be about 35% for the NOCAR ratio and 47% for the GIT ratio. However, the actual uncertainties in the ratio may be smaller, as some of the systematic errors in the individual NO and NO_2 measurements may cancel when the ratio is formed, since both the NOCAR system and GIT system measured ambient NO and photolytically converted NO (from ambient NO_2) using the same procedures (i.e., chemiluminescent in the case of NOCAR and TP-LIF in the case of GIT).

The data from the NOCAR NO and NO_2 instrumentation were generally recorded in 1-min time intervals, while the GIT NO data had resolution varying from 2 to 6 min and the GIT NO_2 data were recorded with 6- to 10-min resolution. Over the entire 8 missions, 74 time intervals were identified with overlapping measurements of NO and NO_2 from both NOCAR and GIT and it is the data gathered during these 74 time intervals upon which our analysis is based. A listing of the mission number, sampling period, and barometric pressure of the air sampled for each time interval is presented in Table 1. Note that the duration of each time interval varied from 6 to 10 min and was chosen to approximately coincide with the sampling period of the lowest-resolution NO_x measurement; i.e., the GIT NO_2 measurement. The NO_2/NO ratios obtained from the NOCAR and GIT measurements along with the observed values for O_3, CO, dew point temperature (T_d), and NO (from NOCAR and GIT) for each time interval are depicted in Figs. 1a through 1g. Each of the ratios indicated in the figures was determined by first averaging the individual NO and NO_2 measurements over the time interval and then dividing the averaged NO_2 by the averaged NO; this approach has been found to yield results that are in close agreement with those obtained from the mathematically exact procedure of first forming the ratio and then averaging over the time interval [Chameides et al., 1987]. The values for O_3, CO, and T_d indicated in the figures were obtained by averaging the 30-s observations recorded for these parameters.

It should be noted that while there was always excellent overlap between NOCAR NO and NO_2 measurements and between the GIT NO and NO_2 measurements, the overlap between the NOCAR and GIT NO_x measurements was more variable. Because of this fact, and because the length of each time interval was chosen to conform to the GIT 6- to 10-min sampling time, many of the time intervals included in our analysis had only partial coverage by the NOCAR measurements. The lack of NOCAR NO_x measurements over the entire sampling period of any given time interval should not have caused significant errors in our analysis as long as the time interval had little or no chemical variability, since the average concentration over a portion of the time interval should be reasonably representative of the average for the entire interval. On the other hand, the lack of complete NOCAR coverage may have given rise to significant errors in our analysis for those intervals which had significant chemical variability. To assess the possible magnitude of this effect, two

TABLE 1. Listing of Time Intervals and Their Mission Numbers, Sampling Times, and Average Pressures

Time Interval	Mission No.	Time (UT)	P, mbar
1	7	2056:51-2104:04	1002
2	7	2107:05-2114:18	1002
3	8	1824:53-1831:06	552
4	8	1850:37-1857:22	553
5	8	1900:34-1906:37	553
6	10	1822:53-1829:13	550
7	10	1828:53-1834:53	550
8	10	1836:37-1843:36	550
9	10	1843:36-1850:15	550
10	10	1917:29-1923:48	679
11	10	1923:29-1929:29	770
12	10	1929:29-1936:26	870
13	10	1938:10-1944:10	987
14	10	1944:10-1950:10	999
15	10	2000:33-2006:33	1000
16	10	2006:33-2013:18	1000
17	10	2014:33-2020:33	1000
18	10	2105:49-2111:53	930
19	10	2122:18-2128:18	930
20	11	1833:19-1839:38	738
21	11	1839:38-1845:57	738
22	11	1847:38-1854:22	738
23	11	1909:26-1916:22	718
24	11	1917:26-1923:47	709
25	11	1923:47-1929:50	632
26	11	1936:24-1942:30	564
27	11	1942:30-1949:02	562
28	11	1950:30-1957:27	561
29	11	2044:33-2051:31	631
30	11	2055:59-2101:59	633
31	11	2101:59-2108:21	633
32	11	2123:10-2129:25	632
33	12	1817:44-1823:44	541
34	12	1823:32-1829:44	540
35	12	1829:44-1836:10	540
36	12	1842:52-1849:48	540
37	12	1850:52-1857:12	541
38	12	2015:00-2021:15	770
39	12	2025:15-2031:50	769
40	12	2034:24-204:36	769
41	12	2043:49-2050:24	769
42	12	2121:41-2128:5	826
43	12	2131:07-2137:2	688
44	12	2137:28-2143:45	612
45	13	1822:45-1829:4	561
46	13	1829:41-1835:44	561
47	13	1837:41-1844:3	561
48	13	1848:22-1855:00	561
49	13	1857:00-1903:00	562
50	13	1955:27-2001:27	566
51	13	2000:58-2007:27	566
52	13	2022:53-2028:53	544
53	13	2030:53-2036:53	540
54	14	1755:10-1802:01	769
55	14	1826:05-1832:49	773
56	14	1834:05-1840:38	770
57	14	1843:39-1849:39	770
58	14	1849:27-1856:18	772
59	14	1857:18-1903:39	772
60	14	1912:56-1919:36	804
61	14	1919:36-1925:47	834
62	14	1927:36-1933:36	778
63	14	1938:43-1944:43	630
64	14	1944:43-1952:15	549
65	14	1959:05-2003:08	465
66	15	1522:37-1533:20	531
67	15	1540:10-1550:00	530
68	15	1550:00-1600:25	531
69	15	1633:58-1644:47	531
70	15	1710:34-1721:22	535
71	15	1819:12-1829:12	530
72	15	1829:12-1839:12	531
73	16	2126:12-2136:12	529
74	16	2301:37-2312:27	529

analyses of the observed ratios will be carried out and discussed later: one which includes all time intervals and another which excludes all intervals that experienced more than a 5 K variation in dew point temperature. Those intervals that had more than a 5 K variation in dew point temperature are identified in Figs. 1a through 1g by an asterisk. During most of these intervals, the aircraft was undergoing an ascent or descent during at least a portion of the sampling period.

Before comparing the observed NO_2/NO ratios, it is interesting to compare the 74 overlapping NO and NO_2 measurements made by the NOCAR and GIT instruments. Scatter plots of NO and NO_2 data are illustrated in Figs. 2 and 3 along with the Pearson-R correlation coefficients calculated from the data sets and the slopes obtained from linear regression of the data. The NO data sets were found to be in excellent agreement. The Pearson-R correlation coefficients of 0.88 for all 74 time intervals and 0.85 for all intervals with NO levels below 30 pptv indicate a high degree of correlation between the two techniques. The slopes obtained from linear regression of the NO data (i.e., 0.79 for all 74 time intervals and 1.02 for time intervals with [NO] less than 30 pptv) also indicate good qualitative agreement in the absolute levels recorded by the two techniques. However, the intercept of about 5 pptv in both cases indicates that the GIT NO tended to be systematically higher than NOCAR NO when [NO] was below about 20 pptv.

Given that the uncertainty in the NO_2 measurements was generally a factor of 1.5 larger than that of NO, it is not surprising that the agreement between the NOCAR and GIT NO_2 measurements was not as good as that of the NO measurements. The relatively high degree of scatter in the NO_2 measurements is apparent from a comparison of Figs. 2 and 3, and this is reflected in the relatively small correlation coefficient of 0.45 calculated for $[NO_2]$ when intervals with levels greater than 50 pptv were omitted from the analysis. Like the NO scattergram, linear regression of the NO_2 data yielded a slope less than unity. However in the NO_2 case, the slope was smaller and more consistently less than unity (i.e., 0.62 for the entire data set and 0.46 for all intervals with $[NO_2]$ less than 50 pptv). Together with the intercept of about 10 pptv, these plots indicate that for $[NO_2] < 20$ pptv, GIT tended to be higher than NOCAR, while for $[NO_2] > 40$ pptv, NOCAR was systematically higher. While it is possible that the small bias in the NO data sets noted above and the more substantial bias in the NO_2 data sets noted here are only artifacts caused by the data selection and averaging techniques adopted in our work and are not a reflection of a real systematic difference in the two techniques, they should nevertheless be borne in mind in the discussion that follows.

Comparison of Observed Ratios

The ratios from the first and second time intervals are depicted in Fig. 1a. The data for these intervals were collected

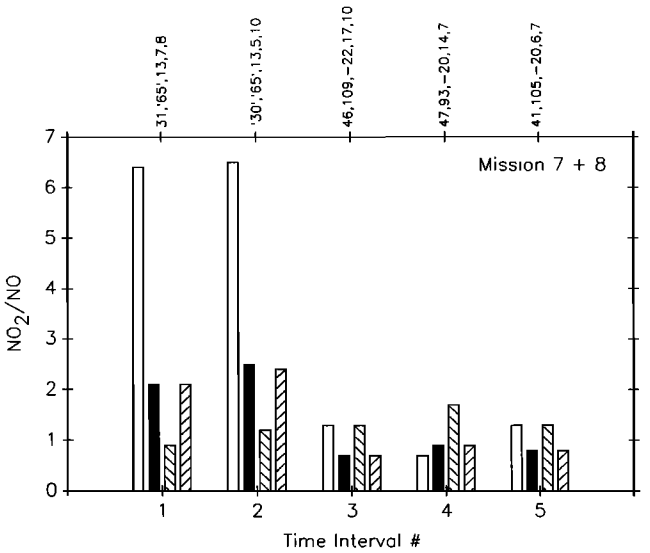

Fig. 1a

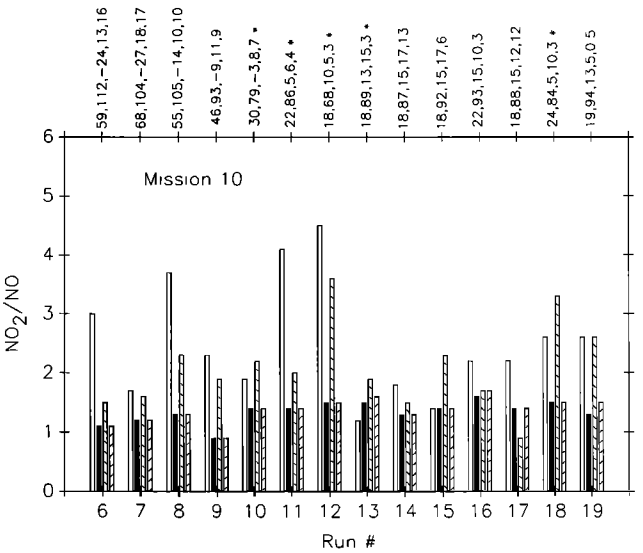

Fig. 1b

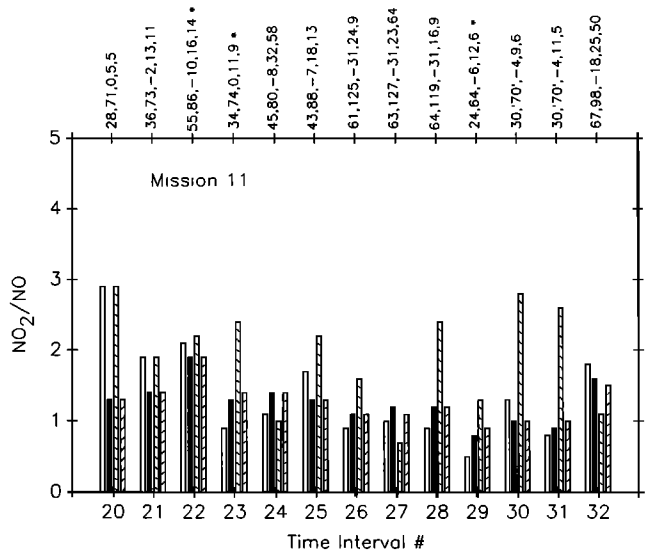

Fig. 1c

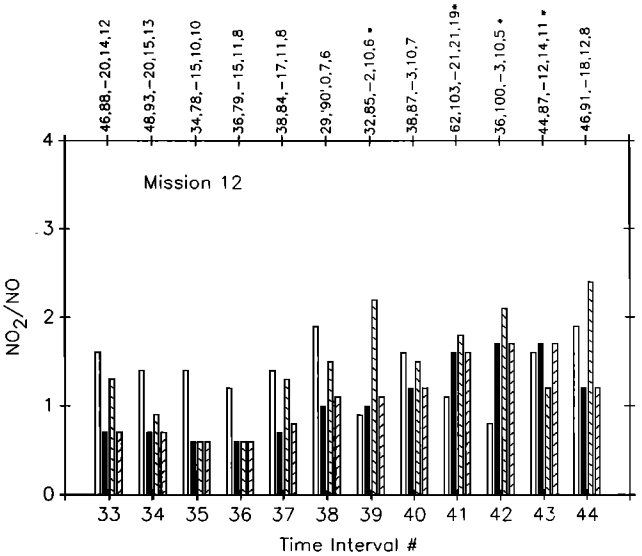

Fig. 1d

Fig. 1. Bar graphs depicting NO_2/NO ratios as a function of time interval: open bar, GIT observed ratio; solid bar, calculated ratio using equation (2) with GIT NO; downward hatched bar, NOCAR observed ratio; and upward hatched bar: calculated ratio using equation (2) with NOCAR NO. Listed along the top in order of appearance are $[O_3]$ (ppbv), [CO] (ppbv), T_d (°C), GIT [NO] (pptv), and NOCAR [NO] (pptv). Asterisks are used to denote time intervals with a variation greater than a 5°C in T_d during the sampling period. Quotations marks are used to denote parameters that were extrapolated. (a) Intervals 1-5, missions 7 and 8; (b) intervals 6-19, mission 10; (c) intervals 20-32, mission 11; (d) intervals 33-44, mission 12; (e) intervals 45-53, mission 13; (f) intervals 54-65, mission 14; and (g) intervals 66-74, missions 15 and 16.

during mission 7 while the aircraft was sampling boundary layer air over the eastern North Pacific Ocean. The NO levels measured by NOCAR and GIT during these two time intervals were in the 5 - 10 pptv range; they agreed in one case nearly exactly and in the other to within a factor of 2. However, because of a much larger discrepancy in the measured NO_2 levels for these two time intervals, the observed NO_2/NO ratios differed by a factor of 6, the largest discrepancy in the observed ratios of the entire data set. By contrast, the ratios observed during time intervals 3, 4, and 5, which had similar levels of NO, are in excellent agreement (see Fig. 1a); the data for these later three time intervals were obtained during mission 8 while the aircraft was sampling mid-tropospheric air over the eastern North Pacific Ocean.

Time intervals 6 through 19 (Fig. 1b) are for data collected during mission 10, another flight over the eastern North Pacific Ocean; as is indicated in Table 1, these data include air sampled in the mid-troposphere and the boundary layer. The NO levels recorded during these time intervals varied from below 5 pptv for the boundary layer data, to values approaching 20 pptv for the free troposphere data. A cursory comparison of the observed ratios does not reveal any obvious pattern with good agreement for some intervals and significant disagreement for others.

Time intervals 20 through 32 cover the data analyzed here from mission 11, a flight over the San Joaquin Valley of California; the data are all from the mid-troposphere, and NO levels in some cases were observed to exceed 30 pptv. Note in

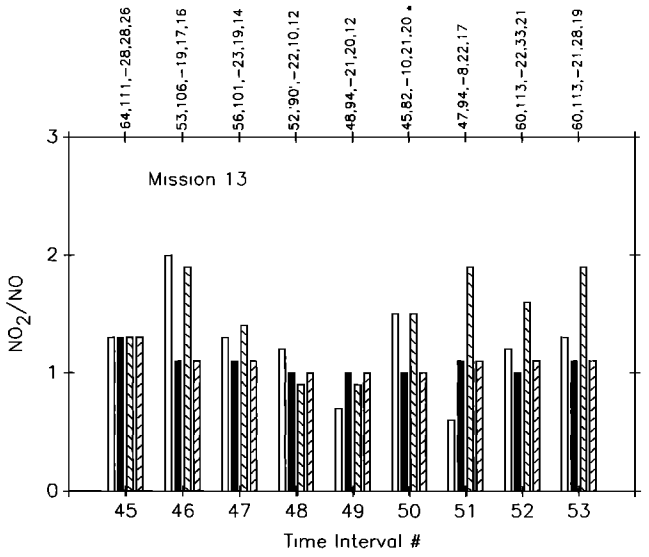

Fig. 1e

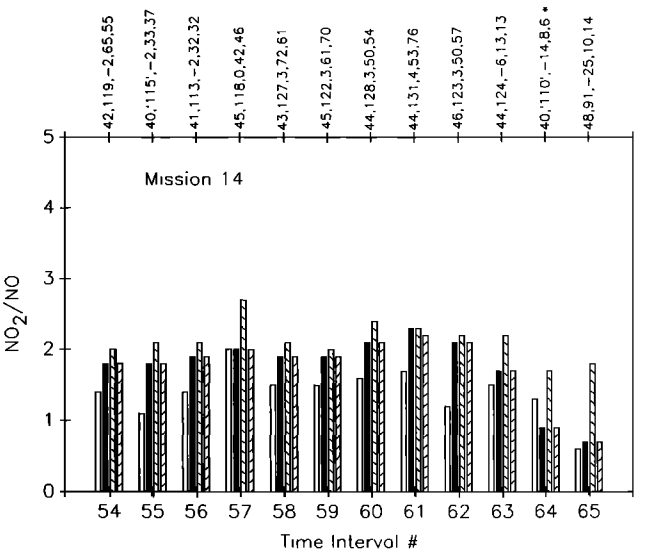

Fig. 1f

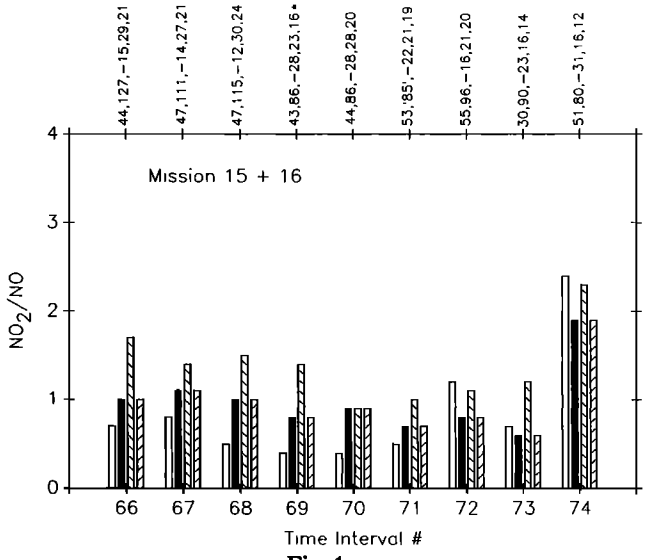

Fig. 1g

Fig. 1, (continued)

Fig. 1c that when the NO levels were the highest (i.e., time intervals 24, 27, and 32), the GIT NO was lower than the NOCAR NO. In contrast to data from later missions with relatively high NO_x levels, the NO_2/NO ratio observed by GIT was larger than that observed by NOCAR for two of these three time intervals.

The data analyzed from mission 12, another flight over the eastern North Pacific Ocean, are covered by time intervals 33 through 44 and are depicted in Fig. 1d. While these data were all obtained from the mid-troposphere (see Table 1), the NO levels remained below 20 pptv. The largest discrepancy between the two observed NO_2/NO ratios for these data occurred during time interval 42 when the NOCAR ratio was found to be a factor of 3 larger than that of GIT; this interval was characterized by large variations in dew point as well as NO and NO_2, and it is possible that the discrepancy is more a reflection of sampling differences in the two techniques than in an actual systematic error in either of the measurements.

Time intervals 45 through 53 depicted in Figure 1e cover the data analyzed here from mission 13, a continental flight over the southwestern United States. All the data for these time intervals were obtained from the mid-troposphere, and the NO levels averaged about 20 pptv. With the exception of time interval 51, when the GIT NO_2/NO ratio was a factor of 3 lower than the NOCAR ratio, the observed ratios from this mission agree quite well. While the data analyzed from mission 14 (i.e., time intervals 54 through 65) were also obtained from the mid-troposphere overlying the southwestern United States, the results contrast sharply with those of mission 13. The NO levels recorded by both GIT and NOCAR were significantly higher than those recorded during mission 13 and exceeded 30 pptv for all but the last three time intervals. Furthermore, the GIT NO_2/NO ratio was found to be less than the NOCAR ratio for all the time intervals analyzed from this mission (see Fig. 1f).

Time intervals 66 through 74 cover the data obtained from missions 15 and 16, when the aircraft was returning to Wallops Island, Virginia from Moffett Field, California. The NO levels during these missions ranged from 15 to 30 pptv and, like mission 14, the GIT observed ratios were less than the NOCAR ratios for all but one of the time intervals analyzed from the two missions.

A scatter plot of the entire set of NOCAR and GIT observed ratios is presented in Fig. 4. The figure indicates a large amount of scatter between the two ratios, with a fairly low correlation coefficient of only 0.18. (Note that the correlation coefficient improved to 0.44 when the two time intervals from mission 7 were omitted from the analysis; the largest discrepancies between the observed ratios were obtained from these two time intervals.) The poor correlation

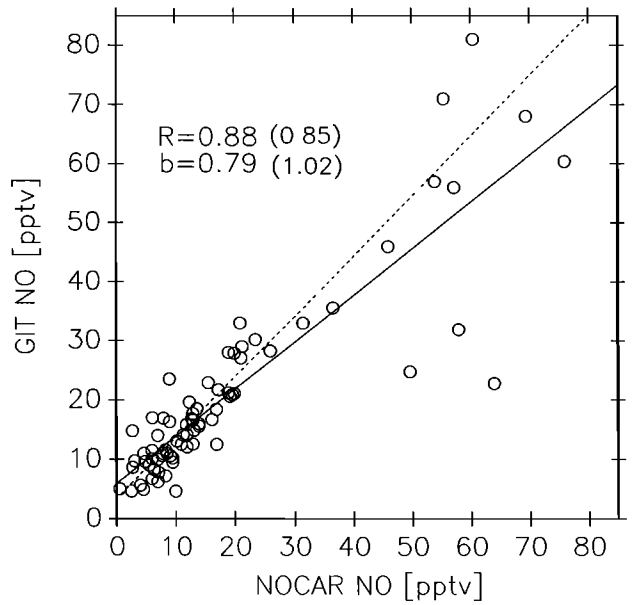

Fig. 2. Scatter plot of GIT NO versus NOCAR NO. The solid line shows linear regression for all data. The dashed line shows linear regression for data with [NO] < 30 pptv. Values for R, the correlation coefficient, and b, the slope, are shown for the entire data set and for the data with [NO] < 30 pptv by the numbers outside and inside the parentheses.

in the observed ratios is perhaps not surprising given the sizeable uncertainties in the NO and NO_2 measurements themselves and the additive effect of these uncertainties upon the random error in the ratios formed from these measurements.

In order to further investigate the source of the discrepancies in the observed ratios consider the observed ratio difference (ORD), defined by

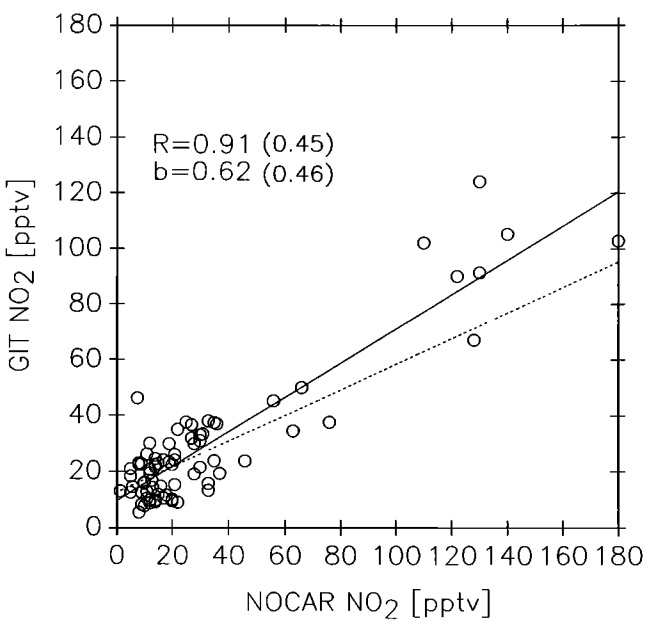

Fig. 3. Scatter plot of GIT NO_2 versus NOCAR NO_2. The solid line shows linear regression for all data. The dashed line shows linear regression for data with $[NO_2]$ < 50 pptv. Values for R, the correlation coefficient, and b, the slope, are shown for the entire data set and for the data with $[NO_2]$ < 50 pptv by the numbers outside and inside the parentheses.

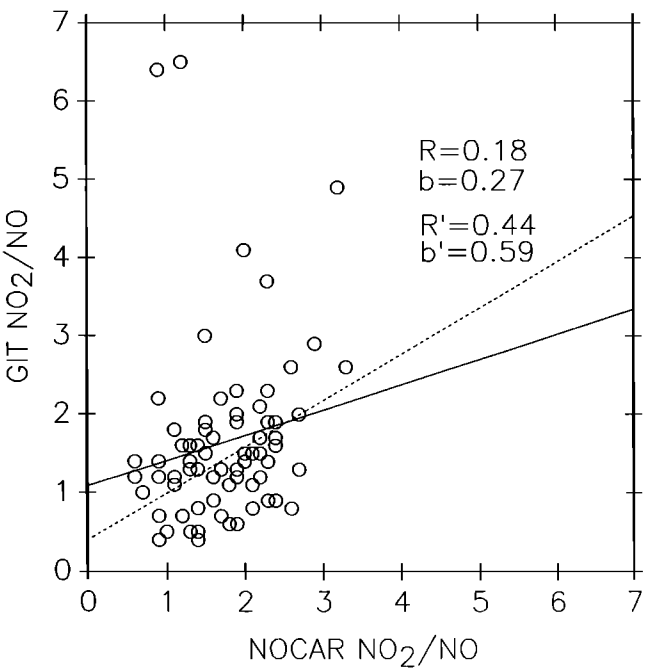

Fig. 4. Scatter plot of GIT observed ratio versus NOCAR observed ratio. The solid line, R, and b indicate linear regression line, correlation coefficient and slope of linear regression line, respectively, for the entire data set. The dashed line, R', and b' indicate linear regression line, correlation coefficient, and slope of linear regression line respectively, for the data without time intervals 1 and 2 from mission 7.

$$\mathrm{ORD} = \frac{\{NO_2/NO\}_{NOCAR} - \{NO_2/NO\}_{GIT}}{\mathrm{MAX}\left[\{NO_2/NO\}_{NOCAR}, \{NO_2/NO\}_{GIT}\right]} \qquad (3)$$

where the function MAX[A,B] is equal to the maximum of the two quantities A and B. (Note that because the maximum observed ratio is used in the denominator of equation (3), ORD is constrained to vary between +1 and -1. ORD values of +0.25, +0.5, and +0.75 occur when the NOCAR ratio is larger than the GIT ratio by factors of 1.33, 2.0, and 4.0, respectively. ORD values of -0.25, -0.5, and -0.75 occur when the NOCAR ratio is smaller than the GIT ratio by factors of 0.75, 0.5, and 0.25, respectively.) The ORD value for any given time interval represents the relative or normalized difference in the two ratios for that time interval and is caused by a combination of random and systematic errors in the two measurements. However, because random errors tend to cancel when individual observations are averaged, the average ORD for the entire data set should reflect only the systematic bias in the two measurements. Thus if the two sets of measurements had no systematic bias, we would obtain an average ORD of zero with a standard deviation characteristic of the random differences.

In Fig. 5, ORD is plotted as a function of time interval; the mean value (+0.12) and 1-σ standard error of the mean (0.04) for all 74 time intervals are also plotted on the far right-hand side of the figure. While a good deal of random scatter is apparent in Fig. 5 with ORD varying from a minimum of -0.85 and -0.82 for the first two time intervals, to a maximum of +0.7 for intervals 31 and 69, the mean ORD is considerably closer to zero. This result suggests that a large fraction of the non zero ORD values in Fig. 5 were caused by the random errors in the instrumentation and sampling rather than by systematic errors and thus that at least on average, the two techniques yielded reasonably consistent NO_2/NO ratios. It is

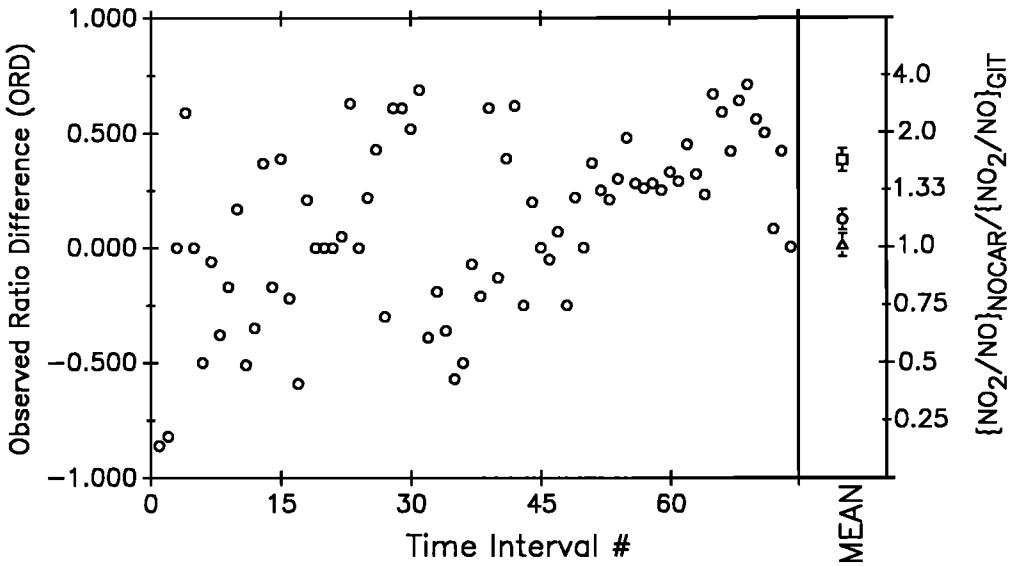

Fig. 5. Observed ratio difference, ORD, (with corresponding ratio of $\{NO_2/NO\}_{NOCAR}$ to $\{NO_2/NO\}_{GIT}$ indicated on righthand vertical axis) as a function of time interval. Mean ratio differences and 1-σ standard error of the means are indicated on the far right for all time intervals (circle), time intervals without missions 14, 15, and 16 (triangle), only time intervals from mission 14, 15, and 16 (square). Note that an ORD value of ±0.5 is indicative of a factor of 2 difference in the two ratios.

also interesting to note that our results do not appear to be dominated by errors related to chemical variability during the individual time intervals; for instance, if we eliminate all the intervals which had more than a 5 K change in dew point temperature over their sampling periods and are indicated by an asterisk in Fig. 1, the mean ORD improves slightly to 0.09.

Some interesting characteristics of the ratio differences are revealed from an inspection of Fig. 6, where the ORD is plotted as a function of NOCAR [NO]. We find that the largest positive and negative ORD values are associated with NO levels of about 20 pptv or less, as one might expect since in this range the NO_x levels are close to the NOCAR and GIT detection limits. However, while most of the discrepancy between the two ratios for low NO levels appears to be random in nature, a more systematic trend is apparent when NO levels exceeded 20 pptv; for these higher NO levels the ORD values are predominantly positive, indicating a tendency for NOCAR ratios to be greater than GIT ratios. Interestingly, closer examination of these time intervals reveals that virtually all of the large positive ORD values obtained when [NO] was greater than 20 pptv were from missions 14, 15, and 16 (see Fig. 6). While it is not clear what factor or factors unique to these missions might have given rise to a systematic discrepancy between the two ratios, it is interesting to note that by eliminating all the data from these three missions, the mean ORD decreases from 12% to only 1%. In contrast, the mean ORD for the time intervals from missions 14, 15, and 16 is +0.38, indicating a factor of 1.6 difference between the NOCAR and GIT observed ratios for these flights. (See Fig. 5 and Table 2).

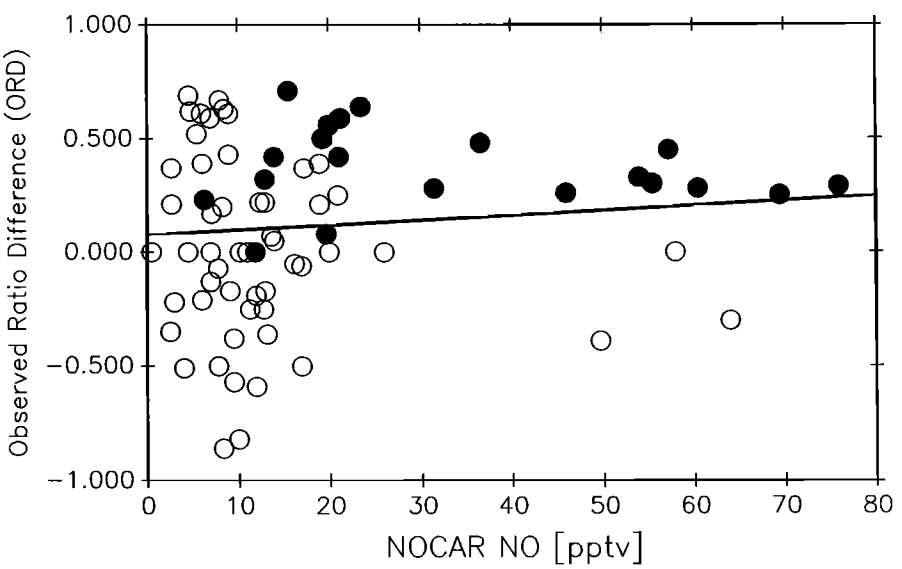

Fig. 6. Observed ratio difference as a function of NOCAR NO. Open circles are from missions 7, 8, 10, 11, 12, and 13, and solid circles are from missions 14, 15, and 16. The solid line indicates linear regression line.

TABLE 2. Mean Ratio Differences, Standard Deviations, and Standard Errors of Means

Ratio Difference	Full Data Set	Data Set Without Missions 14, 15, and 16	Data Set With Only Missions 14, 15, and 16
ORD	+0.12 ±0.38 (0.04)	+0.01± 0.36 (0.05)	+0.38± 0.19 (0.04)
$(CRD)_{GIT}$	+0.38 ±0.32 (0.04)	+0.49± 0.27 (0.04)	+0.01± 0.27 (0.06)
$(CRD')_{GIT}$	+0.09 ±0.36 (0.04)	+0.20 ±0.30 (0.05)	-0.20 ±0.25 (0.05)
$(CRD)_{NOCAR}$	+0.50 ±0.23 (0.03)	+0.50 ±0.25 (0.04)	+0.50± 0.18 (0.04)
$(CRD')_{NOCAR}$	+0.23 ±0.26 (0.03)	+0.23 ±0.30 (0.05)	+0.23± 0.16 (0.04)

Values shown are the mean ratio difference 1-r standard deviations (1-r standard error of the means).

Could the poor agreement between the observed ratios during missions 14, 15, and 16 have been caused by a systematic error in either the NOCAR or GIT NO_2 measurements made during these flights? One way of investigating this possibility is to compare the NOCAR and GIT NO_2 measurements from these flights with those obtained from the YU tunable diode laser absorption spectrometer. (A unique aspect of the the YU system is that it measures NO_2 directly whereas both the NOCAR and GIT systems measure NO_2 through detection of photolytically converted NO.) In Table 3 the NO_2 concentrations recorded from the three different techniques are listed for nine time intervals (54-62) from mission 14. We limited the comparison to these intervals since they had high NO_x levels and were therefore most suitable for an intercomparison involving the YU data. Unfortunately, no firm conclusions can be reached from the data in Table 3. While the YU NO_2 measurements are in better agreement with the GIT measurements during some time intervals, they agree better with the NOCAR measurements during others. Thus no apparent reason for the anomalously poor agreement between the NOCAR and GIT ratios from missions 14, 15, and 16 can be identified at this time.

Calculated NO_2/NO Ratios

While the NO and NO_2 levels were observed to vary by almost 2 orders of magnitude over the 74 time intervals considered, examination of Figures 1a through 1g reveals that the observed NO_2/NO ratios exhibited much less variability, ranging from a minimum of about 0.5 to a maximum of about 6. The fact that the NO_2/NO ratio variability is much less than the variability in either NO or NO_2 suggests that these two species are positively correlated with each other, as one would expect if NO and NO_2 were controlled by a photostationary state relationship of the form of equation (1) or (2). In order to carry out a more quantitative test of photochemical theory, NO_2/NO ratios based on equations (1) and (2) were calculated and compared with the ratios obtained from the GIT and NOCAR measurements, as described below.

In the case of the simple photostationary state relationship (i.e., equation (1)), values for $\{NO_2/NO\}_{pss}$ were calculated for each of the 74 time intervals using the averaged $[O_3]$ and temperature observed during each interval. (The temperature during each time interval was used to determine k_1, using the Arrhenius expression recommended by DeMore et al., [1987].) Values for J_2 were calculated from the UV-Eppley photometer readings recorded during the flights using the semi-empirical formula of Madronich [1987]; i.e.,

$$J_2 = \frac{1.35\,E_u}{(0.56 + 0.03z)\cos\theta + 0.21 - 0.015z} + 2(1.14)E_d \quad (4)$$

where z is altitude (in kilometers), θ is zenith angle, and E_u and E_d are the upward-looking and downward-looking Eppley readings (in megawatts per square centimeter), respectively.

TABLE 3. Comparison of NO_2 Measurements for Time Intervals With Highest NO_x Concentrations

Time Interval	NO_2 Observed Concentrations, pptv		
	NOCAR	GIT	YU
54	110	102	66
55	76	38	63
56	66	46	50
57	122	90	125
58	127	124	100
59	140	105	99
60	130	91	71
61	175	103	66
62	128	67	95

The reader should note, however, that there is some indication that the use of the Eppley readings from the CITE 2 flights to infer values for J_2 may have introduced a systematic error into our calculations. While the Eppley readings upon which Madronich based his formula typically peaked at about 6 mWatts cm^{-2}, the peak readings from the upward-looking Eppley during some of the CITE 2 flights were in excess of 7 mWatts cm^{-2}. While radiative transfer calculations indicate that these large peak Eppley readings could have been caused by cloud albedo effects from clouds positioned over the horizon but out of the line of sight of the sun, it is also possible that the large readings reflect instrumental problems with the UV-Eppley photometers used during the flights. If this later case is true, then the J_2 values inferred from equation (4) and used in our calculations are overestimated by 15-20%.

Values for $\{NO_2/NO\}_{pss}$' (i.e., the modified steady state relationship, equation (2)), require all of the data described above as well as concentrations of peroxy radicals. For the results presented here, we used concentrations of HO_2 and CH_3O_2 radicals obtained from a photochemical box model similar to that described by Chameides et al., [1987, 1989]. The model is based on a chemical mechanism which included the reactions of the H_xO_y-N_xO_y-O_3 system and the CH_4-CO oxidation sequence. (Calculations were also carried out that included the effect of longer chain peroxy radicals (i.e., RO_2) on the NO_2/NO ratios. The RO_2 levels needed for these calculations were estimated from a more detailed photochemical model capable of simulating the oxidation of nonmethane hydrocarbons [Chameides, 1984; Richardson, 1988] which was constrained to yield nonmethane hydrocarbon and peroxyacetyl nitrate (PAN) levels consistent with those observed during the CITE 2 flights [Singh et al., this issue]. The effect of the calculated RO_2 radicals was found to be small; in general, inclusion of RO_2 radicals resulted in only a 10% enhancement in the calculated NO_2/NO ratios over those calculated with only HO_2 and CH_3O_2 radicals.)

In the photochemical box model, the levels of O_3, NO, H_2O, CO, CH_4, and H_2 as well as temperature and pressure are specified, and the concentrations of short-lived species such as HO_2 and CH_3O_2 are calculated assuming photochemical equilibrium. For the calculations presented here, the values used for [O_3], [CO], [NO], dew point temperature, and pressure for each time interval were equal to those observed during the flights. Since the model-calculated peroxy radical concentrations are dependent on [NO], two sets of calculations were carried out for each time interval in order to avoid biasing the calculations in favor of either set of NO_x observations; one set of calculations used NO levels observed by GIT and the other the NOCAR NO levels. Concentrations of CH_4 and H_2 were assumed to be 1.7 and 0.55 ppmv, respectively.

Photolytic rate constants have a strong impact on our calculated NO_2/NO ratios. These rate constants include J_2; the J value for the photolysis of NO_2, which appears explicitly in equations (1) and (2); and a host of others which are input into the photochemical box model and affect the levels calculated for peroxy radicals. The J values used in our calculations of the modified steady state equation were calculated for each time interval using a two-stream radiative transfer model to determine the solar flux for cloud-free conditions as a function of altitude, solar zenith angle, and wavelength [Dickerson et al., 1979;] and an empirically derived scaling factor to include the effect of clouds and other variables not simulated in the radiative transfer model. The scaling factor was assumed to be wavelength independent and was equal to the ratio between the J_2 value calculated using the two-stream model and that calculated using equation (4). The minimum scaling factor obtained for the data set was 0.7; this value was calculated for a boundary layer time interval and probably reflects the influence of overlying clouds. The maximum scaling factor, on the other hand, was 1.6; this value was calculated for a mid-tropospheric time interval and could have been caused by underlying clouds reflecting radiation back up to the aircraft. The average scaling factor for the entire data set was 1.1.

The resulting NO_2/NO ratios calculated for each time interval using GIT and NOCAR NO levels as input to the photochemical box model are indicated in Figures 1a through 1g. The effect of the calculated peroxy radical concentrations on the NO_2/NO ratios is illustrated in Figures 7 and 8, where NO_2/NO ratios calculated from equation (1) and equation (2) are plotted as function of time interval. The modified photostationary state equation was found to be larger than that of the simple photostationary state by a factor of 1.3 to 2. The largest differences were calculated for time intervals such as 1 and 2 with NO levels of 10 pptv or less, relatively high dew

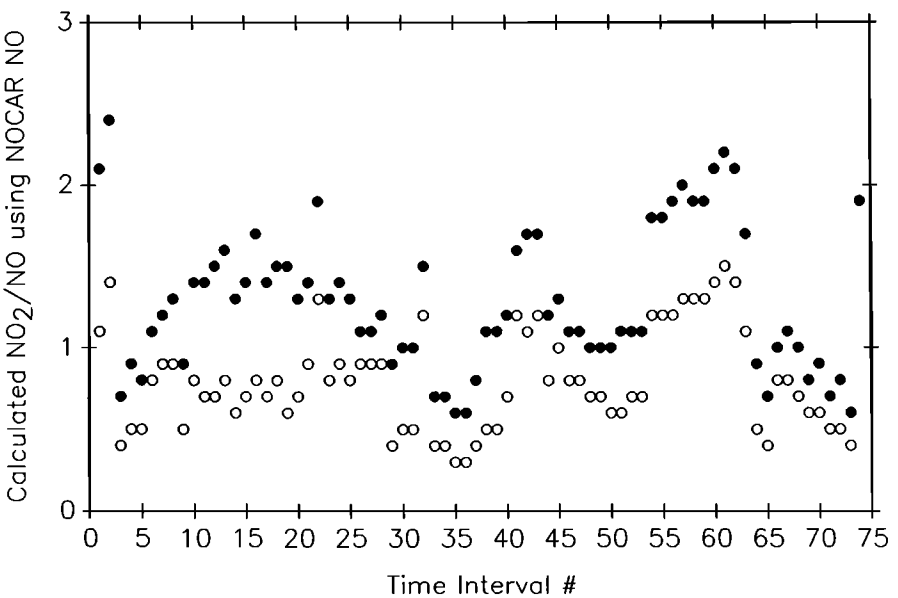

Fig. 7. Calculated NO_2/NO ratio using NOCAR NO as a function of time interval. Open circles denote ratios calculated with equation (1), and solid circles denote ratios calculated with equation (2).

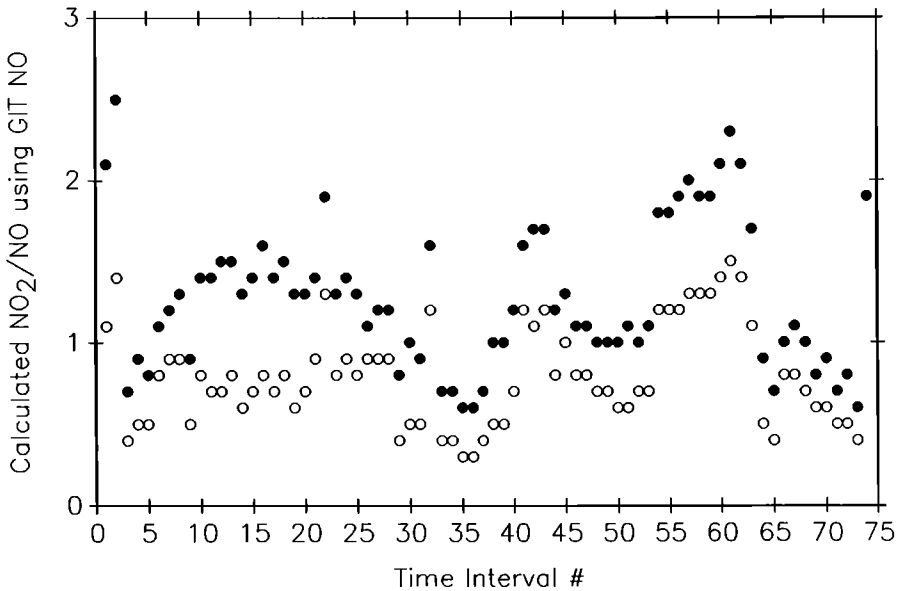

Fig. 8. Calculated NO_2/NO ratio using GIT NO as a function of time interval. Open circles denote ratios calculated with equation (1), and solid circles denote ratios calculated with equation (2).

point temperatures, and O_3 levels of 30 ppbv or less; the low NO and high H_2O concentrations favor larger peroxy radical levels, and the combination of this effect and the low $[O_3]$ causes relatively large rates of conversion of NO to NO_2 by reactions (R4) and (R5) compared with (R1). Conversely, the smaller differences were obtained for time intervals such as 70 characterized by higher levels of NO and O_3 and lower dew point temperatures. An exception to this general trend was found for time interval 74, which had the smallest difference between the two calculated ratios of the entire data set in spite of a relatively modest NO level; however, in this particular case the solar zenith angle was exceptionally large (i.e., 80°) and as a result, radical formation was suppressed.

Comparison of Observed and Calculated Ratios

In Figures 9 and 10 we present scatter plots of calculated and observed NO_2 concentrations from the NOCAR and GIT data sets, respectively. While linear regression of the data in these plots yields slopes reasonably close to unity and high Pearson-r correlation coefficients, some caution should be exercised in interpreting these results. The slopes are dominated by the data points with high NO_2 concentrations and are not representative of the entire data set. In the case of the correlation coefficient it should be borne in mind that the calculated NO_2 is obtained from the product of the observed NO concentration and the calculated NO_2/NO ratio. Since the NO_2/NO ratio is only a weak function of [NO], the high correlation coefficient obtained between the calculated and observed NO_2 is more an indication of the strong correlation between ambient [NO] and $[NO_2]$ rather than a quantitative validation of photochemical theory. Nevertheless, the fact that ambient [NO] and $[NO_2]$ are found to be correlated is consistent with the photostationary state equations and as such represents at least qualitative confirmation of photochemical theory.

As an alternate approach to comparing theory and observations, we define the following four calculated ratio difference (CRD) functions:

$$(CRD)_{GIT} = \frac{\{NO_2/NO\}_{GIT} - \{NO_2/NO\}_{pss}}{MAX\left[\{NO_2/NO\}_{GIT}, \{NO_2/NO\}_{pss}\right]} \quad (5a)$$

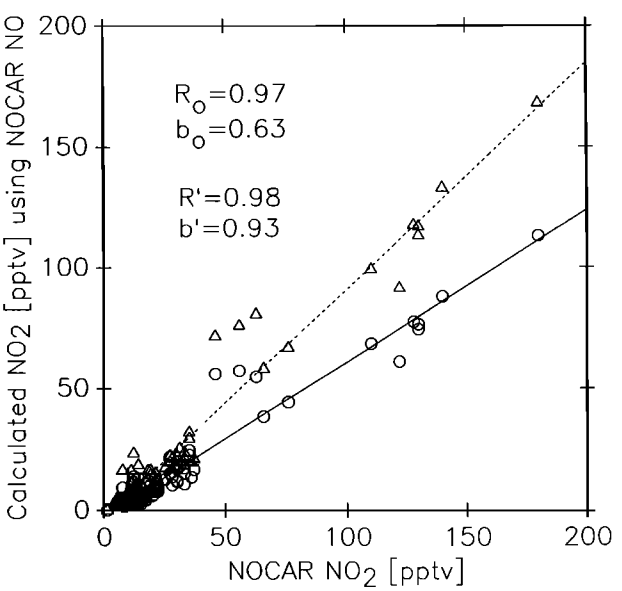

Fig. 9. Scatter plot of calculated $[NO_2]$ (using NOCAR NO observations) and NOCAR observed $[NO_2]$. The circles are for $[NO_2]$ calculated using equation (1) and the triangles are for $[NO_2]$ calculated using equation (2). The solid line, R_0, and b_0 indicate linear regression line, correlation coefficient, and slope of linear regression, respectively, for $[NO_2]$ calculated using equation (1). The dashed line, R', and b' indicate linear regression line, correlation coefficient, and slope of linear regression line, respectively, for $[NO_2]$ calculated using equation (2).

$$(CRD')_{GIT} = \frac{\{NO_2/NO\}_{GIT} - \{NO_2/NO\}_{pss',GIT}}{MAX\left[\{NO_2/NO\}_{GIT}, \{NO_2/NO\}_{pss',GIT}\right]} \quad (5b)$$

$$(CRD)_{NOCAR} = \frac{\{NO_2/NO\}_{NOCAR} - \{NO_2/NO\}_{pss}}{MAX\left[\{NO_2/NO\}_{NOCAR}, \{NO_2/NO\}_{pss}\right]} \quad (5c)$$

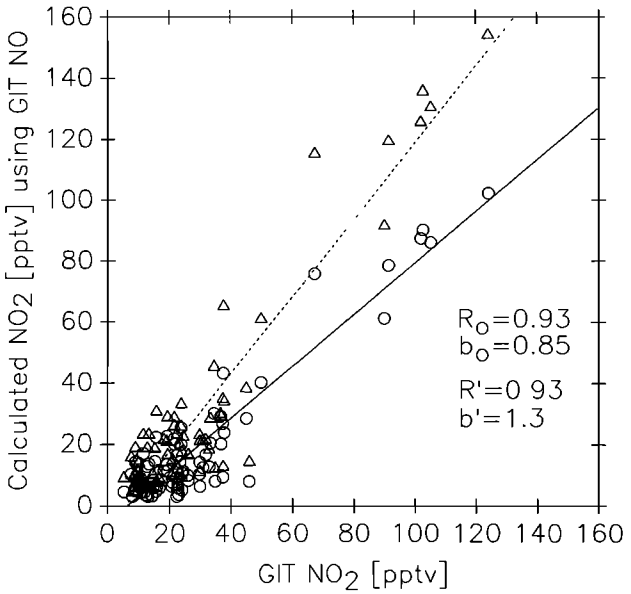

Fig. 10. Scatter plot of calculated $[NO_2]$ (using GIT NO observations) and GIT observed $[NO_2]$. The circles are for $[NO_2]$ calculated using equation (1), and the triangles are for $[NO_2]$ calculated using equation (2). The solid line, R_o, and b_o indicate linear regression line, correlation coefficient, and slope of linear regression, respectively, for $[NO_2]$ calculated using equation (1). The dashed line, R', and b' indicate linear regression line, correlation coefficient, and slope of linear regression line, respectively, for $[NO_2]$ calculated using equation (2).

$$(CRD')_{NOCAR} = \frac{\{NO_2/NO\}_{NOCAR} - \{NO_2/NO\}_{pss',NOCAR}}{MAX\left[\{NO_2/NO\}_{NOCAR},\{NO_2/NO\}_{pss',NOCAR}\right]} \quad (5d)$$

where $(CRD)_{GIT}$ is the fractional difference between the GIT observed ratio and ratio calculated from the simple photostationary state equation, $(CRD')_{GIT}$ is the fractional difference between the GIT observed ratio and the ratio calculated with the modified photostationary state equation using the GIT observed NO, $(CRD)_{NOCAR}$ is the fractional difference between the NOCAR observed ratio and the ratio calculated from the simple photostationary state equation, and $(CRD')_{NOCAR}$ is the fractional difference between the NOCAR observed ratio and the ratio calculated with the modified photostationary state equation using the NOCAR observed NO.

Plots of the four CRD functions versus time interval are presented in Figures 11 and 12. Similar to our comparison of the observed ratios in Fig. 5, we found a large amount of variability in all four CRD functions from one time interval to another, with many intervals having CRD magnitudes in excess of 0.5 (i.e., a factor of 2 discrepancy). However, a large fraction of the discrepancy between the calculated and observed ratios appears to be random rather than systematic. As indicated on the far right hand side of Figures 11 and 12 and in Table 2, the mean calculated ratio differences are within 20-25% of 0 when the modified photostationary state equation was used, implying at least reasonably good agreement between observations and present-day photochemical theory. Furthermore, while the average ratio differences between the GIT observations and the calculations are somewhat smaller than those involving the NOCAR observations when the entire data set is used, the agreement between observations and theory is virtually identical for both sets of ratio measurements when the time intervals from missions 14, 15, and 16 are omitted from the analysis. (Interestingly, the NOCAR CRD functions are not affected by the inclusion or exclusion of the data from the last three missions, while the GIT CRD functions increase significantly when the data from missions 14, 15, and 16 are omitted. In fact, the ratios predicted by equation (2) are actually larger than the ratios observed by the GIT instrumentation during these missions.)

Conclusions

An analysis of two independent sets of airborne NO_y measurements obtained during the NASA GTE/CITE 2 field sampling campaign indicates reasonable agreement between

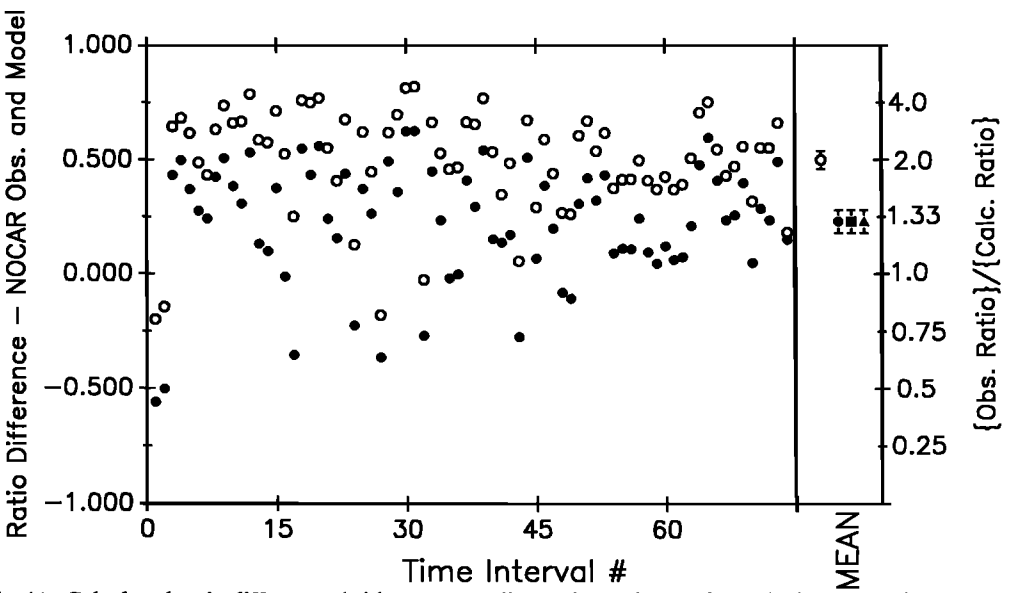

Fig. 11. Calculated ratio difference (with corresponding ratio of observed to calculated NO_2/NO indicated on right-hand vertical axis) using NOCAR observations as a function of time interval. Open circles denote $(CRD)_{NOCAR}$, the NOCAR calculated ratio difference using equation (1). Solid circles denote $(CRD')_{NOCAR}$, the NOCAR calculated ratio difference using equation (2). Mean values and standard errors of the mean are indicated on the right for all time intervals (circles), all time intervals except those from missions 14, 15, and 16 (triangle), and only the time intervals from missions 14, 15, and 16 (square).

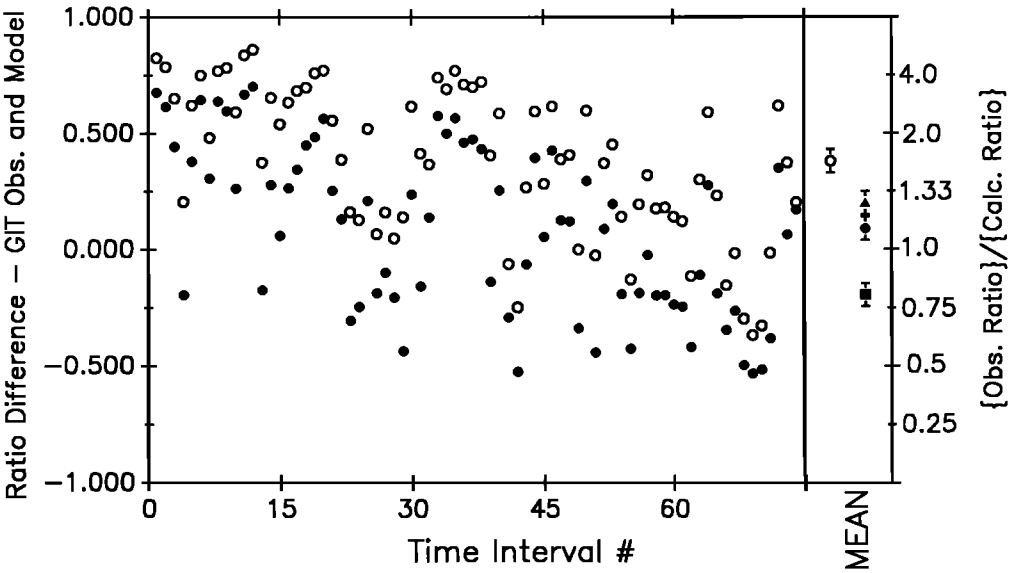

Fig. 12. Calculated ratio difference (with corresponding ratio of observed to calculated NO_2/NO indicated on right-hand vertical axis) using GIT observations as a function of time interval. Open circles denote $(CRD)_{GIT}$, the GIT calculated ratio difference using equation (1). Solid circles denote $(CRD')_{GIT}$, the GIT calculated ratio difference using equation (2). Mean values and standard errors of the mean are indicated on the right for all time intervals (circles), all time intervals except those from missions 14, 15, and 16 (triangle), and only the time intervals from missions 14, 15, and 16 (square).

the NO_2/NO ratios inferred from the observations. While the two ratios were found to differ by a factor of 2 or larger for some 6 to 10 min time intervals with overlapping measurements, the average difference for all time intervals analyzed was only about 10%, with a standard deviation of 40% and a standard error of the mean of 4%. Elimination of anomalous data from three missions, yielded an average ratio difference of only 1% with a similar standard deviation and standard error of the mean. Two important points can be inferred from these results: (1) large random variations are associated with the NO_x measurements, making comparisons of quantities such as the NO_2/NO ratio from individual time intervals statistically meaningless; and (2) with the use of the entire data set, a statistically meaningful comparison can be made, and this comparison indicates reasonable agreement within the stated standard error of the mean.

A comparison of the observed ratios and those calculated based on photochemical theory also indicates reasonably good agreement. In contrast to a number of previous studies of NO_2/NO ratios in nonurban air, there was no evidence of a large systematic trend with model-calculated ratios falling far below the observed ratios. The better agreement between observations and theory in the case of the CITE 2 data base is likely due, at least in part, to the techniques used by the GIT and NOCAR instruments to convert NO_2 to NO when measuring NO_2 levels; these techniques appear to be more specific to NO_2 than techniques used by other investigators and as a result the GIT and NOCAR NO_2 measurements are probably less influenced by artifacts arising from other NO_y compounds [cf., Gregory et al., this issue (b)].

However, while our analysis appears to qualitatively confirm present-day photochemical theory, there is still evidence for a small, but statistically significant discrepancy between model-calculated and observed NO_2/NO ratios. On average, model-calculated ratios using the modified photostationary state equation are about 25% smaller than the observed ratios; the standard deviation of the mean for both data sets is only about 5%. While this discrepancy could easily have been caused by an error either in the NO_x measurements or in the model-calculated peroxy radical concentrations or some combination of the two, it could just as easily have been caused by a 25% over- estimation of the J_2 values from equation (4). Thus a more stringent test of model-predicted peroxy radical conversion of NO to NO_2 will likely require accurate NO_2-actinometric measurements as well as NO_x measurements.

Acknowledgments. This work was supported in part by funds from the National Aeronautics and Space Administration (NASA) under grants NAG-1-385 and NAG-1-50 and from the National Science Foundation under 8208828 and ATM-8600888. We thank Roger Navarro, the flight crew, and the maintenance personnel of the NASA Wallops Island Flight Facility responsible for the Electra aircraft. We also thank the personnel at the NASA Ames Research Center for providing facilities for ground-based operations as well as flight support. Partial support was provided by the NASA Tropospheric Chemistry Program to M.A.C. and B.A.R. The National Center for Atmospheric Research is sponsored by the National Science Foundation.

References

Cadle, R. D., and H. S. Johnston, Chemical reactions in Los Angeles smog, Proc. Natl. Air Pollut. Symp., 2nd, 1952.

Calvert, J. G., and W. R. Stockwell, Deviations from the O_3-NO-NO_2 photostationary state in tropospheric chemistry, Can. J. Chem., 61, 983-992, 1983.

Chameides, W. L., and D. D. Davis, Iodine: Its possible role in tropospheric chemistry, J. Geophys. Res., 85, 7383-7398, 1980.

Chameides, W. L., The photochemistry of a remote marine stratiform clouds, J. Geophys. Res., 89, 4739-4755, 1984.

Chameides, W. L., D. D. Davis, G. L. Gregory, G. Sachse, and A. L. Torres, Ozone precursors and ozone photochemistry over eastern North Pacific ocean during the spring of 1984 based on the NASA GTE/CITE 1 airborne observations, J. Geophys. Res., 94, 9799-9808, 1989.

Chameides, W. L., D. D. Davis, M. O. Rodgers, J. D. Bradshaw, S. Sandholm, G. Sachse, G. Hill, G. L. Gregory, and R. Rasmussen, Net ozone photochemical production over the eastern and central North Pacific as inferred from

GTE/CITE 1 observations during fall 1987, J. Geophys. Res., 92, 2131-2152, 1987.

DeMore, W. B., M. J. Molina, S. P. Sander, D. M. Golden, R. F.Hampson, M. J. Kurylo, C. J. Howard, and A. R. Ravishankara, Chemical kinetics and photochemical data for use in stratospheric modeling, Evaluation #8, JPL Publ. 87-41, 196 pp, Jet Propul. Lab., Pasadena, Calif., 1987.

Dickerson, R. R., D. D. Stedman, W. L. Chameides, P. J. Crutzen, and J. Fishman. Actinometric measurements and theoretical calculations of $J(O_3)$, the rate of photolysis of ozone to $O(^1D)$, Geophys. Res. Lett., 6, 833-837, 1979.

Fehsenfeld, F. C., M. J. Bollinger, S. C. Liu, D. D. Parrish, M. McFarland, M. Trainer, D. Kley, P. C. Murphy, D. L. Albritton, and D. H. Lenschow, A study of ozone in the Colorado mountains, J. Atmos. Chem., 1, 87-105, 1983.

Gregory, G. L., J. M. Hoell, Jr., M. A. Carroll, B. A. Ridley, D. D. Davis, J. Bradshaw, M. O. Rodgers, S. T. Sandholm, H. I. Schiff, D. R. Hastie, D. R. Karecki, G. I. MacKay, G. W. Harris, A. L. Torres, and A. Fried, An intercomparison of airborne nitrogen dioxide instruments, J. Geophys. Res., this issue (a).

Gregory, G. L., J. M. Hoell, Jr., A. L. Torres, M. A. Carroll, B. A.Ridley, M. O. Rodgers, J. Bradshaw, S. T. Sandholm, and D. D. Davis, An intercomparison of airborne nitric oxide measurements: A second opportunity, J. Geophys. Res., this issue (b).

Hoell, J. M., Jr., D. L. Albritton, G. L. Gregory, R. J. McNeal, S. M. Beck, R.J. Bendura, and J. W. Drewry, Operational overview of NASA GTE/CITE-2 airborne instrument intercomparisons: Nitrogen dioxide, nitric acid, and PAN, J. Geophys. Res., this issue.

Leighton, P. A., Photochemistry of Air Pollution, Academic Press, New York, 300 pp, 1961.

Madronich, S., Intercomparison of NO_2 photodissociation and U.V. radiometer measurements, Atmos. Environ., 21, 569-578, 1987.

McFarland, M., D. Kley, and J. W. Drummond, Simultaneous NO, NO_2, and O_3 vertical profile measurements from ground level to 6 km, paper presented at the 4th Biennial Rocky Mountain Regional Meeting, Am. Chem. Soc., Boulder, Colo., June 1978.

Parrish, D. D., M. Trainer, E. J. Williams, D. W. Fahey, G. Hubler, C. S. Eubank, S. C. Liu, P. C. Murphy, D. L. Albritton, and F. Fehsenfeld, Measurements of the NO_x-O_3 photostationary state at Niwot Ridge, Colorado, J. Geophys. Res., 91, 5361-5370, 1986.

Richardson, J. L., The role of biogenic hydrocarbons in the photochemical production of tropospheric ozone in the Atlanta, Georgia Region, M.S. thesis, Ga. Inst. of Technol., Atlanta, 1988.

Ridley, B. A., M. A. Carroll, G. L. Gregory, and G. W. Sachse, NO and NO_2 in the troposphere: Technique and measurements in regions of a folded tropopause, J. Geophys. Res., 93, 15,803-15,812, 1988.

Ritter, J. A., D. H. Stedman, and T. J. Kelly, Ground-level measurements of nitric oxide, nitrogen dioxide and ozone in rural air, in Nitrogenous Air Pollutants: Chemical and Biological Implications, edited by D. Grosjean, Butterworth, Stoneham, Mass., 1979.

Sandholm, S. T., K. S. Dorris, M. O. Rodgers, D. D. Davis, and J. Bradshaw, An airborne compatible photofragmentation two-photon laser induced fluorescence instrument for measuring background tropospheric levels of NO, NO_x, and NO_2, J. Geophys. Res., this issue.

Schiff, H. I., D. R. Karecki, G. W. Harris, D. R. Hastie, and G. I. MacKay, A tunable diode laser system for aircraft measurements of trace gases, J. Geophys. Res., this issue.

Singh, H. B., D. O'Hara, E. Condon, J. Vedder, B. A. Ridley, B. W. Gandrud, J. D. Shetter, L. J. Salas, B. Huebert, G. Huebler, M. A. Carroll, D. L. Albritton, D. D.Davis, J. D. Bradshaw, S. T. Sandholm, M. O. Rodgers, S. M. Beck, G. L. Gregory, and P. J. LeBel, PAN measurements during CITE 2: Atmospheric distribution and precursor relationships, J. Geophys. Res., this issue.

Stedman, D. H., and J. O. Jackson, The photostationary state in photochemical smog, Int. J. Chem. Kinetics, Symp. 1, 493-501, 1975.

Torres, A., Nitric oxide measurements at a nonurban eastern United States site: Wallops instrument results from July 1983 GTE/CITE Mission, J. Geophys. Res., 90, 12875-12880, 1985.

Trainer, M., E. Y. Hsie, S. A. McKeen, R. Tallamraju, D. D. Parrish, F. C. Fehsenfeld and S. C. Liu, Impact of natural hydrocarbons in hydroxyl and peroxy radicals at a remote site, J. Geophys. Res., 92, 11879-11894, 1987.

B. Baum, J. Bradshaw, W. L. Chameides, D. D. Davis, M. Rodgers, and S. Sandholm, School of Earth and Atmospheric Sciences, Georgia Institute of Technology, Atlanta, GA 30332.

M. A. Carroll, NOAA, R/E/AL6, Boulder, CO 30303.

E. Condon, Atmospheric Experiments Branch, NASA Ames Research Center, Moffett Field, CA 94305.

G. Gregory, NASA Langley Research Center, Hampton, VA 23665.

D. R. Hastie and H. I. Schiff, Department of Chemistry, York University, Downsiew, Ontario, Canada M3J 1P3.

S. Madronich and B. Ridley, NCAR, P.O. Box 3000, Boulder, CO 80307.

A. Torres, NASA Wallops Flight Center, Wallops Island, VA 23337.

(Received August 28, 1989;
revised January 22, 1990;
accepted January 23, 1990.)